

MALAYSIAN JOURNAL OF ANALYTICAL SCIENCES



Journal homepage: https://mjas.analis.com.my/

Research Article

Optimisation studies and synthesis of a surface-modified-Samanea saman-based carbon adsorbent with copper ions for gliclazide removal

Mohd Raziff Mat Hasan, Erniza Mohd Johan Jaya, and Mohd Azmier Ahmad*

School of Chemical Engineering, Engineering Campus, Universiti Sains Malaysia, 14300 Nibong Tebal, Penang, Malaysia

*Corresponding author: chazmier@usm.my

Received: 6 May 2025; Revised: 4 August 2025; Accepted: 5 August 2025; Published: 25 August 2025

Abstract

This study investigates the potential of copper (Cu²⁺)-modified Samanea saman-derived carbon adsorbent (Cu²⁺-SSAC) for the removal of gliclazide (GLI), a pharmaceutical contaminant, from aqueous solutions. The pristine SSAC exhibited an adsorption capacity of 50.52 mg/g, which significantly increased to 71.69 mg/g following Cu²⁺ ion modification representing a 41.90% enhancement in adsorption efficiency. This improvement is attributed to the increased number of active sites and the enhanced surface properties resulting from Cu2+ incorporation. The Cu2+-SSAC exhibited a Brunauer-Emmett-Teller surface area (BET-SA) of 752.25 m²/g, a mesoporous surface area (MESO-SA) of 550.85 m²/g, a total pore volume (TPV) of 0.3074 cm³/g, and an average pore diameter of 2.43 nm. Scanning electron microscopy (SEM) analysis revealed a notable development of surface pores in Cu²⁺-SSAC compared to the precursor material, highlighting the effectiveness of the carbonisation and activation processes employed. Optimisation using response surface methodology (RSM) determined the ideal conditions as an activation temperature of 587 °C, an activation time of 1.09 h, and a Cu²⁺ ion impregnation ratio (IR) of 0.50 g/g. Under these conditions, the predicted GLI adsorption capacity and Cu²⁺-SSAC yield were 70.13 mg/g and 32.33%, respectively. These values closely matched the experimental results of 71.69 mg/g and 33.42%, with low relative errors of 2.17% and 3.26%. Isotherm analysis indicated that GLI adsorption onto Cu²⁺-SSAC followed the Langmuir model, with a maximum adsorption capacity (Qm) of 109.21 mg/g. The Freundlich heterogeneity factor (n_F) was 1.73, shows a favourable adsorption behaviour. These findings demonstrate the practical potential of Cu²⁺-SSAC as a cost-effective and sustainable adsorbent for mitigating pharmaceutical pollutants in wastewater treatment applications.

Keywords: adsorption process, surface modification, activated carbon, optimisation, isotherm

Introduction

Pharmaceutical compounds are recognised as emerging micropollutants that can disrupt aquatic ecosystems by affecting flora and fauna and may also pose potential risks to human health when present in water bodies. Studies have indicated that even at trace concentrations, pharmaceutical compounds can compromise water safety and disrupt the ecological balance over time [1]. Up to 90% of pharmaceutical compounds are excreted from the human body through urine and faeces due to incomplete intestinal absorption, and these excreted compounds can enter the environment through the application of untreated sewage sludge or animal manure, leading to their accumulation in agricultural waste or discharge into wastewater systems [2]. When used in human medicine, these compounds often make their way

into the wastewater and sludge generated by treatment plants (WWTPs). However, many WWTPs are not equipped to adequately remove or degrade pharmaceutical compounds, leading to their persistent presence in effluent discharges and accumulation in the treatment sludge. Gliclazide is a commonly used pharmaceutical compound with antidiabetic properties. It is listed, along with metformin and insulin, in the World Health Organisation's (WHO) 2021 Model List of Essential Medicines as a key medication for the management of diabetes [3].

Numerous technologies have been employed to eliminate pharmaceutical compounds from wastewater, each offering distinct advantages and limitations. Among these, adsorption which relies on the surface interaction mechanism, has emerged as a particularly effective method due to its versatility in capturing a wide range of contaminants, including heavy metals [4], pharmaceutical compounds [5], synthetic dyes [6], antibiotic [7], and carbon dioxide, CO₂ gas [8]. This method is favoured for its straightforward operation, high removal efficiency, and economic viability [9]. Traditionally, the activated carbon (AC) used in adsorption is sourced from coal, a non-renewable material associated with environmental concerns and high production costs. In response, researchers are increasingly turning to agricultural byproducts, such as rice husks [10], Alpinia galanga stem [11], and biomass sludge [12], as sustainable alternatives for AC production.

Improving AC production has recently gained attention due to the many factors affecting its efficiency. Response surface methodology (RSM) offers a powerful statistical tool for optimising multiple variables and modelling processes effectively [13]. Among the RSM methods, central composite design (CCD) is widely used because it minimises experimental runs, reveals variable interactions, and builds predictive models. Three-dimensional (3D) plots illustrate parameter effects, while analysis of variance (ANOVA) validates model accuracy and significance [14].

AC adsorbs contaminants through its large surface area and active sites. Improving its porosity often requires high heat, long processing, and more chemicals, increasing costs. To overcome this, researchers added metals to the AC, forming a metalsurface-modified AC, which enhanced performance without complex processing. Positively charged metals attract pollutant groups. Copper (Cu²⁺) is widely used because of its strong binding affinity towards various functional groups and its ability to form stable surface complexes, which enhance the adsorption process [2]. Additionally, it offers a cost-effective alternative to noble metals such as platinum or silver, while still providing performance excellent in water treatment applications due to its redox activity and relatively low toxicity [15]. Using a low-toxicity metal minimizes the secondary pollution risk, making the adsorbent safer for practical applications. Furthermore, Cu2+ has been successfully used to modify AC to enhance the removal of pharmaceutical pollutants. In one study, Cu2+-modified lemon peelbased AC increased amoxicillin adsorption by 38.93% [2], while in another study, Cu²⁺-modified rattan waste-based AC improved chloramphenicol removal by 30.40% [15].

In this study, Samanea saman wood was used as a precursor to produce Samanea saman-based AC

(SSAC), which was further modified with Cu²⁺ ions to form copper-modified SSAC (Cu²⁺-SSAC) for the adsorption of gliclazide (GLI) from aqueous solutions. Samanea saman waste has been proven to be a promising precursor for AC, demonstrating excellent potential for removing pollutants from water. In one study, Samanea saman was chemically activated to produce AC that successfully adsorbed hexavalent chromium, attributed to its high porosity [16]. In another study, Samanea saman waste-based AC was effectively utilised to adsorb copper ions [17]. However, research on Samanea saman-based AC for the removal of pharmaceutical pollutants remains limited, underscoring the relevance of this study. The synthesis conditions of Cu2+-SSAC were systematically optimised using Response Surface Methodology (RSM). Samanea saman was selected because of its wide availability in Malaysia as a fastgrowing, underutilised biomass with lignocellulosic content, making it a sustainable and cost-effective raw material for carbon-based adsorbent production.

Materials and Methods Precursor, chemicals, and gases

Raintree wood, specifically from the limb of *Samanea saman*, was collected from the International Islamic University Malaysia, Gombak, Selangor, and used as the primary precursor material. Gliclazide (GLI) in powdered form (purity >98%) and copper nitrate, Cu(NO₃)₂ (purity 99.99%), were obtained from Sigma-Aldrich. High-purity nitrogen (N₂) and carbon dioxide (CO₂) gases (99.99% purity) were supplied by MOX Gases Berhad, Malaysia.

Synthesis of Cu2+-SSAC

The raw precursor was initially rinsed thoroughly with water to eliminate surface dirt and impurities. It was then cut and ground into small pieces measuring approximately 1-1.5 cm. The material was ovendried at 60 °C for 24 h before being weighed and transferred into a vertical furnace. Pyrolysis was carried out at 550 °C for 2 h under a continuous N2 flow to produce char. The resulting char was subsequently activated using CO2 at varying activation temperatures (432-768 °C) and activation durations (0.32–3.68 h). CO₂ was chosen as the activating agent because it offers greater control over the activation process and minimises excessive burnoff, thereby preserving the AC yield [18]. This process yielded the pristine SSAC. Surface modification was performed by impregnating the pristine SSAC with Cu2+ ions using copper nitrate, Cu(NO₃)₂, across a range of impregnation ratios (IR) from 0 to 2.51 g/g [2, 15]. The specific experimental conditions for the activation temperature, activation time, and IR were designed using RSM and are presented in Table 1. In the Cu²⁺ impregnation

process, a weighed amount of Cu(NO₃)₂ (e.g., 2.51 g for IR = 2.51 g/g) was dissolved in 100 mL of deionised water to prepare the impregnating solution. Then, 1.00 g of pristine SSAC was added to the solution. The mixture was stirred at 80 rpm for 4 h at room temperature to ensure the uniform adsorption of Cu²⁺ ions onto the SSAC surface. After impregnation, the slurry was oven-dried at 110 °C for 24 h to remove moisture and promote strong adherence of Cu²⁺ onto the SSAC surface. No washing step was performed to retain Cu²⁺ on the surface, which is critical for enhancing the GLI adsorption performance. The IR was calculated using Equation 1:

$$IR\left(\frac{g}{g}\right) = \frac{W_{Cu}(g)}{W_{p}(g)} \tag{1}$$

where W_{Cu} refers to the weight of $Cu(NO_3)_2$ salt and W_p refers to the weight of the precursor.

Optimisation investigation

To optimise the process, the dataset was analysed using the Design Expert software (version 12, STAT-EASE Inc., Minneapolis, USA). A central composite design (CCD) under response surface methodology (RSM) was applied to evaluate the effects of three independent variables: activation temperature (X₁), activation time (X₂), and impregnation ratio (IR, X₃). Two primary responses were examined: adsorption capacity for gliclazide (GLI) (Y1) and the yield of Cu²⁺-modified SSAC (Y₂). The yield refers to the percentage of the mass of Cu2+-SSAC obtained relative to the mass of the original precursor. The experimental design included five levels for each variable: $+\alpha$, +1, 0, -1, and - α , corresponding to activation temperatures of 432, 500, 600, 700, and 768 °C; activation times of 0.32, 1.00, 2.00, 3.00, and 3.68 h; and IR values of 0.00, 0.50, 1.25, 2.00, and 2.51 g/g. Representative studies reporting similar ranges were consulted during experimental planning [19, 20], although specific values were fine-tuned based on preliminary trials using Samanea saman as the precursor. The yield of Cu2+-SSAC was calculated using Equation 2:

$$Yield (\%) = \frac{W_{Cu^2 + -SSAC}}{W_p}$$
 (2)

where $W_{\text{Cu}2+\text{-SSAC}}$ is the dry weight of $\text{Cu}^{2+}\text{-SSAC}$, and W_p refers to the dry weight of the precursor.

Characterisation methods

The study characterised the physicochemical properties of the samples, focusing on the surface area (measured through BET analysis), mesoporosity, pore size distribution, and total pore volume. These parameters were analysed using a Micromeritics

ASAP 2010 volumetric adsorption system. Elemental analysis was performed using a Perkin Elmer Series II 2400 analyser (USA) to determine the sample composition. The proximate analysis was performed using a Perkin Elmer STA 6000 simultaneous thermal analyser (USA) based on thermogravimetric analysis (TGA). In addition, the surface morphology and structural details were visualised using scanning electron microscopy (SEM) with a Quanta 450 FEG instrument (Netherlands). The functional groups on the sample surface were characterised by Fourier Transform Infrared Spectroscopy (FTIR) using a Shimadzu Prestige 21 (Japan).

Adsorption isotherm investigation

Batch adsorption experiments were performed to investigate the equilibrium behaviour of GLI adsorption onto Cu2+-SSAC. Six Erlenmeyer flasks, each containing 200 mL of the GLI solution at initial concentrations (Co. mg/L) of 10, 20, 40, 60, 80, and 100 mg/L, were agitated in a water bath shaker at 30 °C until equilibrium. The temperature of 30 °C was selected to simulate typical ambient conditions relevant to tropical wastewater environments and is also commonly adopted in previous adsorption studies for comparative purposes. The adsorbent dosage (W, g) was fixed at 0.20 g per flask. The concentration of GLI at equilibrium (Ce, mg/L) was at 232 nm using a UV-Vis spectrophotometer (Agilent Cary 60, USA). The equilibrium adsorption capacity (qe, mg/g) was then calculated using Equation 3:

$$q_e = \frac{(c_o - c_e)V}{W} \tag{3}$$

The experimental data were inspected with several models, and the corresponding equations for each model are described by equations (4)–(6):

Langmuir [21]:
$$q_e = \frac{Q_m K_L C_e}{1 + K_L C_e}$$
 (4)

Freundlich [22]:
$$q_e = K_F C_e^{1/n_F}$$
 (5)

Temkin [23]:
$$q_e = \frac{RT}{R} \ln(AC_e)$$
 (6)

where Q_m and K_L represent the maximum monolayer adsorption capacity (mg/g) and the Langmuir constant related to adsorption affinity (L/mg), respectively; K_F and n_F correspond to the Freundlich constant indicative of adsorption capacity ((mg/g)(L/mg)^(1/n)) and the heterogeneity factor (dimensionless), respectively; and B and A are parameters from the Temkin model associated with adsorption heat (L/mg) and the Temkin equilibrium binding constant (L/mg), respectively [24].

Results and Discussion Optimisation process

Regression model development

Table 1 outlines the full experimental framework, encompassing the variables and responses involved in producing Cu²⁺-SSAC, as determined using RSM. The GLI adsorption capacity was observed to range

from 50.52 to 76.51 mg/g, whereas the material yield varied between 21.47% and 39.71%. Quadratic models based on actual and coded variables were selected by the software, offering reliable mathematical predictions of the outcomes from the respective input parameters, as detailed below:

$$Y_1 = -134.0024 + 0.587952X_1 - 5.19753X_2 + 28.93046X_3 + 0.011538X_1X_2 - 0.03445X_1X_3 + 1.36167X^2X^3 - 0.000422X_1^2 - 1.50434X_2^2 - 2.80951X_3^2$$
(7)

Cu²⁺-SSAC yield (%), Y₂ (Actual):

$$Y_2 = 92.6157 - 0.13486X_1 + 3.31657X_2 - 22.76774X_3 - 0.006625X_1X_2 + 0.0108X_1X_3 + 1.27333X^2X^3 + 0.000075X_1^2 + 0.228467X_2^2 + 3.91970X_3^2$$

$$(8)$$

GLI uptake (mg/g), Y₁ (Coded):

$$Y_{1} = 73.70 + 6.18X_{1} - 2.59X_{2} + 2.97X_{3} + 1.15X_{1}X_{2} - 2.58X_{1}X_{3} + 1.02X^{2}X^{3} - 4.22X_{1}^{2} - 1.50X_{2}^{2} - 1.58X_{3}^{2}$$

$$(9)$$

Cu²⁺-SSAC yield (%), Y₂ (Coded):

$$Y_2 = 27.18 - 4.48X_1 + 1.85X_2 - 2.96X_3 - 0.6625X_1X_2 + 0.81X_1X_3 + 0.955X^2X^3 + 0.7482X_1^2 + 0.2285X_2^2 + 2.20X_3^2$$
(10)

Table 1. Variables and responses for Cu²⁺-SSAC production as generated by the RSM

	Cu ²⁺ -SSAC Pre	Resp	onses		
Run	Activation Temperature, X ₁ (°C)	Activation Time, X ₂ (minutes)	IR, X ₃ (g/g)	GLI Uptake, Y1 (mg/g)	Cu ²⁺ -SSAC Yield, Y ₂ (%)
1	600 (0)	2.00(0)	2.51 (+α)	73.87	27.94
2	500 (-1)	3.00 (+1)	2.00 (+1)	63.11	35.00
3	500 (-1)	1.00 (-1)	2.00 (+1)	68.65	26.76
4	600 (0)	2.00(0)	1.25(0)	74.57	25.59
5	700 (+1)	3.00 (+1)	0.50 (-1)	70.23	28.53
6	700 (+1)	3.00 (+1)	2.00 (+1)	73.42	25.00
7	500 (-1)	1.00 (-1)	0.50 (-1)	59.21	37.35
8	600 (0)	2.00(0)	1.25(0)	74.50	26.76
9	600 (0)	2.00(0)	1.25(0)	76.51	30.88
10	600 (0)	$3.68 (+\alpha)$	1.25(0)	64.18	32.06
11	700 (+1)	1.00 (-1)	0.50 (-1)	75.24	26.76
12	600 (0)	2.00(0)	1.25(0)	75.87	28.53
13	432 (-α)	2.00(0)	1.25(0)	51.31	37.94
14	600 (0)	2.00(0)	1.25(0)	71.15	26.18
15	600 (0)	2.00(0)	1.25(0)	69.75	25.00
16	600 (0)	2.00(0)	$0.00 (-\alpha)$	63.66	39.71
17	500 (-1)	3.00 (+1)	0.50 (-1)	50.52	37.94
18	768 (+a)	2.00(0)	1.25 (0)	71.30	21.47
19	600 (0)	$0.32 (-\alpha)$	1.25 (0)	73.78	24.41
20	700 (+1)	1.00 (-1)	2.00 (+1)	73.41	23.24

Figures 1(a) and 1(b) display the regression plots that compare the predicted versus actual values for the GLI uptake and Cu²⁺-SSAC yield, respectively. The R² and adjusted R² values were 0.9648 and 0.9332 for the GLI uptake and 0.9311 and 0.8692 for Cu²⁺-SSAC yield, reflecting an excellent model fit that accounts for most of the response variability with high statistical reliability. The low standard deviations (S.D.), recorded at 2.00 for the GLI uptake and 1.98 for the yield, confirm the models' precision, stability, and minimal prediction error across all runs. Adequate precision (A.P.) values were 17.51 for GLI uptake and 13.26 for Cu²⁺-SSAC yield, both well above the minimum benchmark of 4, indicating strong signal-to-noise ratios and affirming the models' robustness, reliability, and effectiveness in predicting outcomes across the tested experimental design space [25].

Analysis of variance

Table 2 presents a detailed summary of the analysis of variance (ANOVA) results for the GLI uptake and Cu2+-SSAC yield. Both responses demonstrated strong statistical significance, with p-values of < 0.0001 for GLI uptake and 0.0001 for yield, indicating the reliability of the developed models. For GLI uptake, the significant model terms identified were X_1 , X_2 , X_3 , X_1X_3 , X_1^2 , X_2^2 , and X_3^2 . In the case of Cu2+-SSAC yield, the significant variables included X₁, X₂, X₃, and X₃². The F-values further highlight that both GLI uptake and Cu2+-SSAC yield were predominantly influenced by the activation temperature and IR. Specifically, GLI uptake showed a strong dependence on the activation temperature (130.62) and IR (30.15), while Cu²⁺-SSAC yield was similarly affected by the activation temperature (69.94) and IR (30.42). These results underscore the pivotal role of these two parameters in optimising both adsorptive performance and the material yield.

Three-dimensional (3D) surface plot

Figure 2(a) displays a 3D surface plot illustrating the effects of the activation temperature and IR on the GLI uptake, while **Figure 2(b)** depicts the influence of the same variables on Cu²⁺-SSAC yield. The maximum GLI uptake of 76.51 mg/g was observed at a higher activation temperature of 650 °C and an IR of 1.40 g/g. The elevated temperature facilitated the removal of the volatile matter, promoting pore development and increasing the surface area, which

collectively enhanced the adsorption capacity [26]. It also contributed to the decomposition of light hydrocarbons, resulting in a higher degree of carbonisation and more defined porosity [27]. A higher IR led to an increased concentration of Cu²⁺ ions on the adsorbent surface, strengthening the interactions with the GLI molecules.

In contrast, the lowest GLI uptake of 50.52 mg/g was recorded under the minimum studied conditions of 500 °C and 0.50 g/g. These suboptimal settings restricted pore formation and reduced the availability of surface-bound Cu²⁺, thus resulting in a less effective interaction with GLI. Additionally, activation temperatures above 650 °C caused pore collapse and reduced the surface area, resulting in a slight decline in GLI uptake [28]. Similarly, an IR beyond 1.40 g/g led to excessive Cu²⁺ loading, where surplus metal ions agglomerated on the carbon surface and within the pore channels. This accumulation caused pore blockage and reduced the number of accessible active sites, thereby hindering further adsorption of GLI [15].

Figure 2(b) shows that the minimum SSAC yield of 21.47% was observed at the highest activation temperature and IR, indicating the harmful impact of these parameters on the yield. As the activation temperature increased from 500 to 700 °C, intensified pyrolytic cracking occurred, resulting in substantial elemental loss from the sample and ultimately reducing the yield [14]. Similarly, an increase in IR introduced more Cu2+ ions, which enhanced the burn-off and contributed to the reduction in the carbon yield. At higher IR levels, the excess Cu²⁺ ions catalysed thermal degradation of the carbon matrix and promoted tar volatilisation, resulting in greater carbon loss. This trend has been widely reported, where increased IR intensifies the release of volatiles and carbon burn-off due to the action of excess activating agents [29]. In contrast, the highest yield of 38.54% was obtained at an activation temperature of 500 °C and IR of 0.50 g/g. These results highlight the need for careful adjustment of both the activation temperature and an IR to achieve high yield without compromising the material's functional integrity.

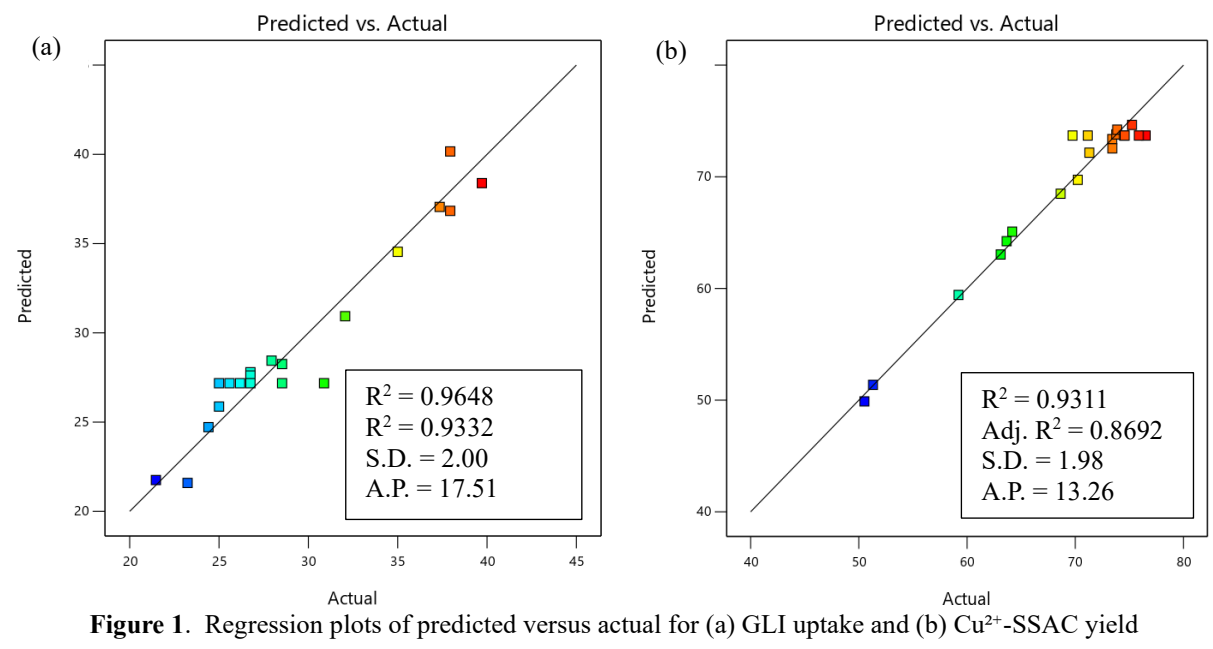
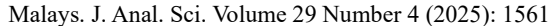


Table 2. ANOVA results for GLI uptakes and Cu^{2+} -SSAC yield responses

Source	Response 1, Y1 (mg/g): GLI uptakes by Cu2+-SSAC							
Source	Sum of the Squares	DF	Mean Square	F Value	p-value			
Model	1096.58	9	121.84	30.49	< 0.0001			
X_1	521.95	1	521.95	130.62	< 0.0001			
X_2	91.63	1	91.63	22.93	0.0007			
X_3	120.47	1	120.47	30.15	0.0003			
X_1X_2	10.65	1	10.65	2.67	0.1336			
X_1X_3	53.41	1	53.41	13.37	0.0044			
X_2X_3	8.34	1	8.34	2.09	0.1791			
X_1^2	256.38	1	256.38	64.16	< 0.0001			
X_2^2	32.61	1	32.61	8.16	0.0170			
X_3^2	35.99	1	35.99	9.01	0.0133			

Source	Response 2, Y ₂ (%): Cu ²⁺ -SSAC yield								
Source	Sum of the Squares	DF	Mean Square	F Value	p-value				
Model	530.59	9	58.95	15.03	0.0001				
X_1	274.42	1	274.42	69.94	< 0.0001				
X_2	46.59	1	46.59	11.87	0.0063				
X_3	119.36	1	119.36	30.42	0.0003				
X_1X_2	3.51	1	3.51	0.8949	0.3665				
X_1X_3	5.25	1	5.25	1.34	0.2743				
X_2X_3	7.30	1	7.30	1.86	0.2026				
X_{1}^{2}	8.07	1	8.07	2.06	0.1821				
X_2^2	0.7522	1	0.7522	0.1917	0.6708				
X_3^2	70.06	1	70.06	17.85	0.0018				



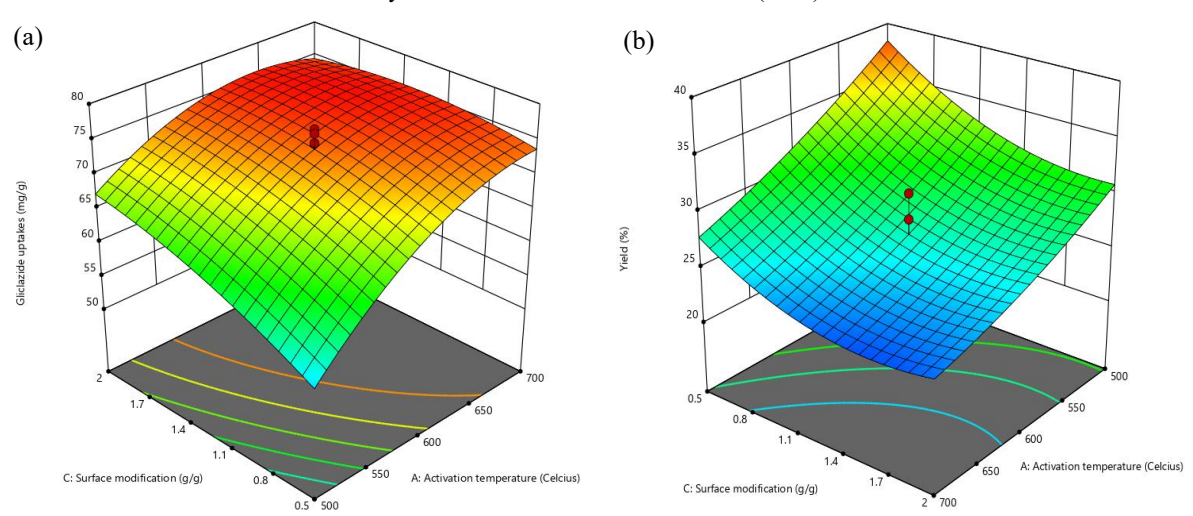


Figure 2. 3D surface plots for (a) GLI uptake and (b) Cu²⁺-SSAC yield responses

Optimal conditions and model validation

Table 3 shows the optimum conditions and model validation. The optimal process conditions were established by minimising input variables while simultaneously maximising the target responses. Using RSM, the predicted optimum values were 587 °C for the activation temperature, 1.09 h for the activation time, and 0.50 g/g for IR. Although the model recommended an activation time of 1.09 h (equivalent to 1 h, 5 min, and 24 s), the validation experiment was practically conducted for 1 h and 5 min to ensure experimental feasibility. These settings yielded predicted responses of 70.13 mg/g for GLI uptake and 32.33% for Cu²⁺-SSAC yield. The corresponding experimental values were 71.69 mg/g and 33.42%, respectively, resulting in low error margins of 2.17% and 3.26%. This close agreement (error below 10%) confirms the reliability and predictive accuracy of the developed statistical models [30].

Characteristics of the samples Surface area and pore characteristics

Table 4 presents the surface and porosity characteristics of the precursor, pristine SSAC, and Cu²⁺-SSAC samples. The precursor exhibited a low Brunauer–Emmett–Teller surface area (BET-SA) of 4.11 m²/g and a total pore volume (TPV) of 0.0001 cm³/g, indicating minimal porosity. During carbonisation, dehydration and the release of light volatile components—primarily cellulose and hemicellulose—initiated pore development. Further pore formation was promoted during physical activation at elevated temperatures, where the decomposition of more compact volatiles, such as hemicellulose-lignin complexes, occurred.

Simultaneously, the interaction with CO₂ gas facilitated the widening and proliferation of the pores [31]. As a result, the pristine SSAC demonstrated a substantial increase in porosity, achieving a BET-SA of 763.85 m²/g, a mesopore surface area (MESO-SA) of 564.21 m²/g, a TPV of 0.3086 cm³/g, and an average pore diameter (APD) of 2.45 nm, indicative of a mesoporous structure. Following surface modification with Cu(NO₃)₂, the BET-SA, MESO-SA, TPV, and APD of the Cu²+-SSAC slightly decreased to 752.25 m²/g, 550.85 m²/g, 0.3074 cm³/g, and 2.43 nm, respectively. This minor reduction is attributed to the partial pore blockage and surface coverage by the deposited Cu salts.

The textural properties of the Cu²⁺-SSAC were assessed through N2 adsorption-desorption analysis at 77 K. The isotherm, as shown in Figure 3(a), exhibited a classical Type IV profile with a pronounced hysteresis loop at higher relative pressures $(P/P_0 > 0.4)$, which is characteristic of mesoporous materials. This observation was further supported by the pore size distribution curve obtained using the Barrett-Joyner-Halenda (BJH) method, as given in Figure 3(b), which revealed a dominant pore diameter centered around 2.43 nm. This value aligns closely with the APD derived from the BET data. The material exhibited a high BET surface area of 752.25 m²/g and a TPV of 0.3074 cm³/g, with Meso-SA contributing 550.85 m²/g. These findings confirm the successful synthesis of a mesoporous adsorbent with a high surface area and well-developed pore structure, which are favorable characteristics for enhancing the adsorption performance of pharmaceutical contaminants in aqueous environments.

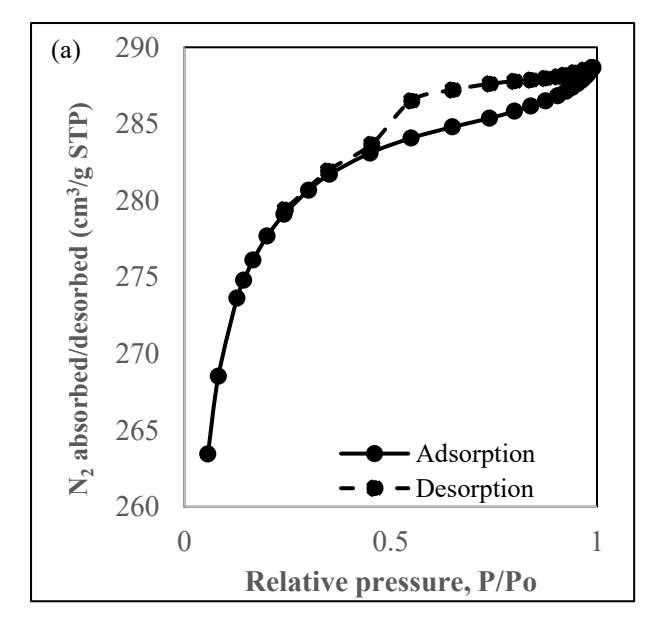
Table 3. Optimum conditions and model validation

Onti	mum vaniah	los	Optimum responses					
Opui	mum variab	oies	GLI uptake, Y ₁			Cu ²⁺ -SSAC yield, Y ₂		
X ₁ (°C)	$X_2(h)$	X ₃ (g/g)	Predicted (mg/g)	Actual (mg/g)	Error (%)	Predicted (%)	Actual (%)	Error (%)
587	1.09	0.50	70.13	71.69	2.17	32.33	33.42	3.26

 X_1 = activation temperature; X_2 = activation time; X_3 = IR

Table 4. Surface area and pore characteristics

Samples	BET-SA (m ² /g)	MESO-SA (m²/g)	TPV (cm ² /g)	APD (nm)
Precursor	4.11	-	0.0001	-
Pristine SSAC	763.85	564.21	0.3086	2.45
Cu ²⁺ -SSAC	752.25	550.85	0.3074	2.43



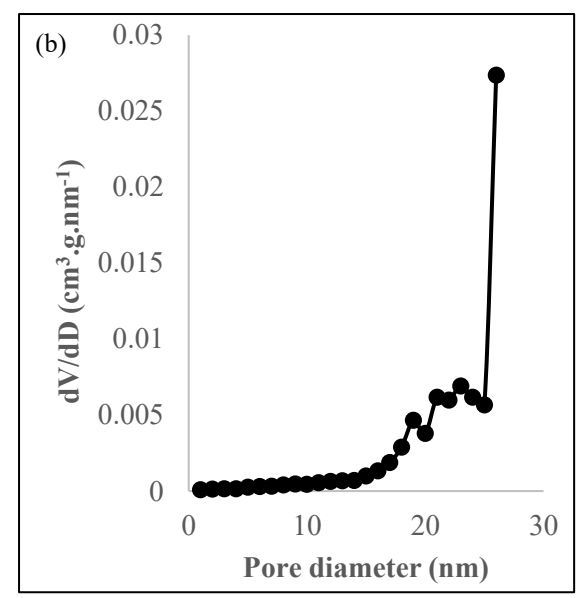


Figure 3. The plots of (a) N₂ adsorption-desorption isotherm and (b) BJH pore size distribution curve

Elemental and proximate analysis

Table 5 presents the consolidated outcomes of the proximate and elemental analyses for the studied samples. Samanea saman exhibited a notably high fixed carbon content of 27.61%, surpassing other biomass sources such as rice husk (13.82%), corn straw (14.12%), wood dust (14.46%), and coconut shell (18.86%) [32]. This supports its justified selection as the precursor material for Cu2+-SSAC in this research. Initially, the precursor displayed elevated levels of moisture and volatile matter, which were reduced to 3.41% and 14.75%, respectively, following carbonisation and activation. Meanwhile, the fixed carbon content increased significantly to 77.24%. The final ash content in the resulting Cu^{2+} -SSAC remained low at 4.60%, which is beneficial because ash does not contribute to adsorption [33].

The elemental analysis mirrored these trends, with the carbon content rising from 37.71% in the raw precursor to 78.55% post-treatment. Conversely, elements linked to volatiles and moisture such as hydrogen, nitrogen, sulfur, and oxygen declined due to their removal during thermal processing.

TGA plot

The thermal stability and decomposition behaviour of the precursor and Cu²⁺-SSAC were evaluated using simulated TGA profiles derived from the proximate analysis data, as shown in **Figure 4**. The mass loss was estimated within three main thermal zones: moisture release (<150 °C), volatilisation of light compounds (150–400 °C), and decomposition of fixed carbon (400–700 °C). The final residue represents the ash content remaining after pyrolysis.

The precursor exhibited the highest mass loss across the temperature range due to its elevated volatile matter content (56.51%) and relatively low fixed carbon content (27.61%). This indicates a weaker thermal resistance and higher degradation potential at mid-range temperatures. In contrast, Cu2+-SSAC demonstrated significantly enhanced stability, attributed to its high fixed carbon content (77.24%) and reduced volatile matter (14.75%). The lower mass loss across the heating profile reflects a more robust and carbon-rich structure, which is essential for maintaining the material integrity under thermal stress. The presence of copper species did not notably alter the decomposition pattern, shows that the modification process preserved the carbon framework while potentially enhancing adsorptive functionality.

SEM images

Figure 5 displays the SEM micrographs of the prepared samples, highlighting their morphological evolution. In **Figure 5(a)**, the surface of the raw *Samanea saman* precursor appears dense and structurally compact, with an absence of discernible pores. This morphology is typical of untreated lignocellulosic biomass, primarily due to the intact matrix of lignin, cellulose, hemicellulose, and tar-like substances.

Figure 5(b) shows the pristine SSAC produced after carbonisation and CO₂ activation. A noticeable transformation in the surface texture was observed compared to the raw precursor. The structure becomes more fragmented, with the appearance of initial pore formation and surface roughening. This morphological change reflects the partial decomposition of the organic constituents and the creation of the basic porosity induced by CO₂ activation, although the pore structure remains less developed than its Cu²⁺-modified counterpart [31].

Finally, **Figure 5(c)** shows that the optimised Cu²⁺-SSAC exhibits a well-developed porous architecture characterised by interconnected cavities and channels. These pores were initially filled with volatile compounds and moisture, which were subsequently eliminated during pyrolysis and CO₂ activation. The removal of these constituents, along with the structural rearrangement induced by the thermal treatment and Cu²⁺ modification, resulted in a significantly enhanced surface area and pore accessibility, which is favourable for adsorption applications.

Samples	E	lement	al Ana	lysis (%	(6)	Proximate Analysis (%)				
Samples	C	Н	N	S	*O+	Moisture	Volatile matter	Fixed carbon	Ash	
Precursor	37.71	5.67	0.91	0.31	55.4	12.61	56.51	27.61	3.27	
Pristine SSAC	80.13	4.29	0.72	0.25	14.61	3.45	14.89	77.45	4.21	
Cu ²⁺ -SSAC	78.55	4.27	0.68	0.24	16.26	3.41	14.75	77.24	4.60	

Table 5. Elemental and proximate analysis of the samples

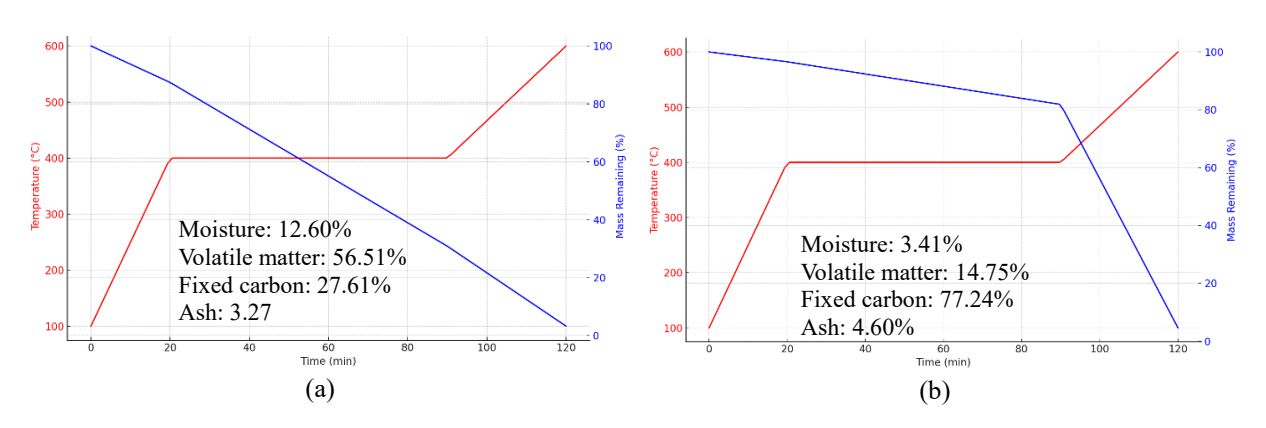
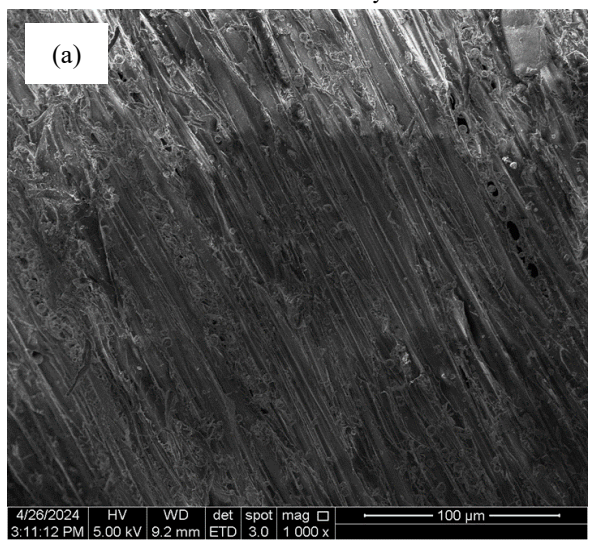
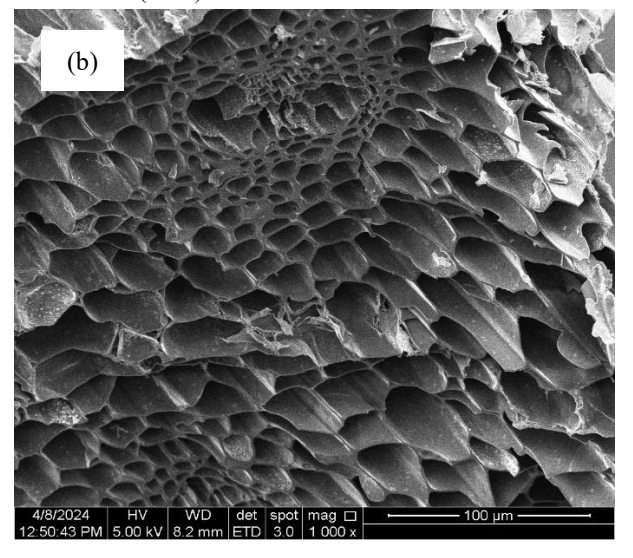


Figure 4. Simulated TGA plot for (a) the precursor and (b) Cu²⁺-SSAC





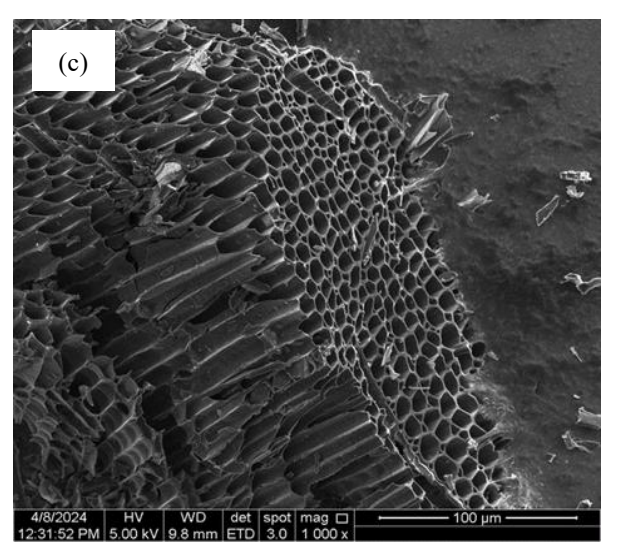


Figure 5. SEM images of (a) the precursor, (b) pristine SSAC , and (c) Cu^{2+} -SSAC (1000× magnification level)

FTIR spectra

The FTIR spectra of the precursor, pristine SSAC, and Cu²⁺-SSAC are presented in **Figure 6**, illustrating the evolution of the surface functional groups throughout the preparation and modification process. For the precursor, several key peaks were observed, including 881.47 cm⁻¹ (substituted alkenes or aromatics), 1026.13 cm⁻¹ (C–O stretching in alcohols or ethers), 1246.02 cm⁻¹ (C–N stretching in amines), 1327.03 cm⁻¹ (aromatic amines), 2860 cm⁻¹ and 2920.23 cm⁻¹ (C–H stretching in alkanes and methyl groups), and a broad band at 3275 cm⁻¹ (O–H stretching from hydroxyl groups).

In the pristine SSAC spectrum, the following peaks were identified: 738.74 cm⁻¹ (aromatic C–H bending), 1029.99 cm⁻¹ (alcohols/ethers), 1246.02 cm⁻¹ (amines), 1348.24 cm⁻¹ (C–N stretching), 1579

cm⁻¹ (C=C stretching in aromatic rings), 2561–2927 cm⁻¹ (thiol, S-H stretching), and 3200–3600 cm⁻¹ (broad O-H and N-H stretching, indicating hydroxyl and amine groups).

Upon copper modification, the Cu²⁺-SSAC spectrum showed distinct or shifted peaks at 746.45 cm⁻¹ (aromatic C–H bending), 1031.92 cm⁻¹ (C–O stretching in alcohols/ethers), 1317.38 cm⁻¹ (C–N or phenolic C–O), 1585.49 cm⁻¹ (C=C in aromatics), and 1969.32 cm⁻¹ (methyl carbonyl group, Cu²⁺coordinated). A broad absorption in the region of 2532–3199 cm⁻¹ further confirmed the presence of O–H, N–H, and S–H stretching vibrations.

These functional groups are believed to play a crucial role in the adsorption mechanism of GLI. The peak at 1969.32 cm⁻¹ indicates ion-dipole interaction

between Cu²⁺ ions and the NH–SO₂ group of GLI. Dipole–dipole interactions occur between the C–O groups at 1031.92 cm⁻¹ and the SO₂ moiety of GLI. Hydrogen bonding is also supported by the peaks at 746.45 cm⁻¹ (aromatic interactions), 3199 cm⁻¹ (N–H···N), and 2561–2927 cm⁻¹ (S–H···O), all contributing to the enhanced GLI adsorption on the Cu²⁺-modified SSAC surface.

Adsorption isotherm

Table 6 presents a comprehensive summary of the fitted isotherm model parameters, while **Figure 7** shows the isotherm plots. Among the tested models, the Langmuir isotherm yielded the best fit for GLI

adsorption onto Cu²⁺-SSAC, as evidenced by the lowest root mean square error (RMSE) value of 0.70 and a minimal error percentage of 3.83%. This superior fit shows that the adsorption follows a monolayer mechanism, likely governed by specific interactions between the GLI molecules and the immobilised Cu²⁺ ions on the SSAC surface. The heterogeneity factor, n_F, ranged from 1 to 10, indicating a favourable and efficient adsorption process. Furthermore, the maximum adsorption capacity, Q_m, reached an impressive 109.21 mg/g, which is considerably higher than that of magnetic multiwalled carbon nanotubes reported for GLI removal of 71.59 mg/g [34].

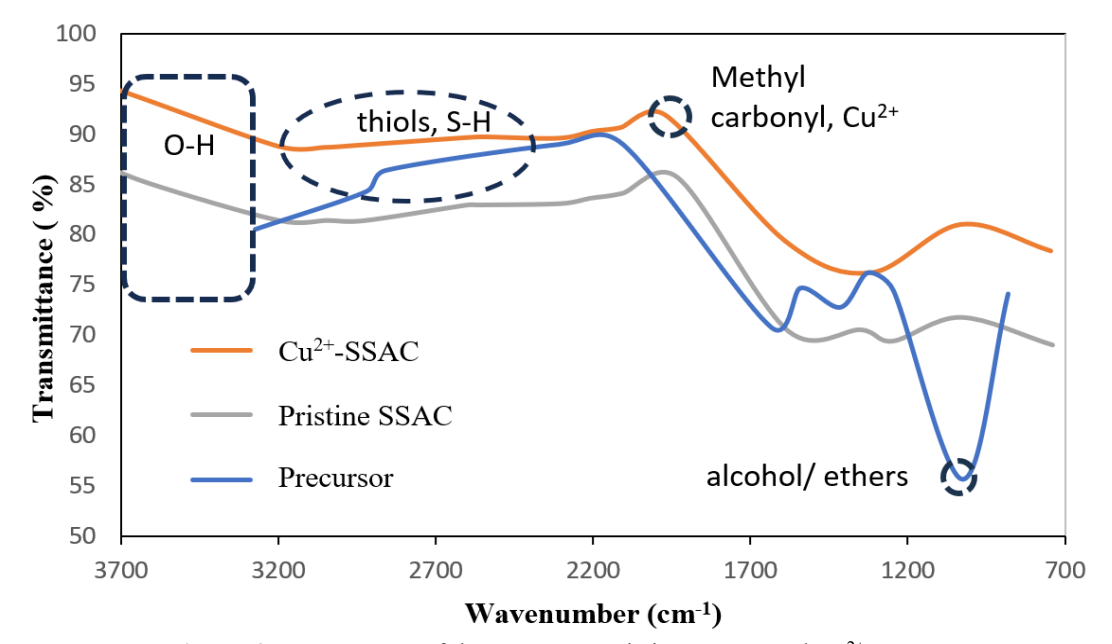


Figure 6. FTIR spectra of the precursor, pristine SSAC, and Cu²⁺-SSAC

Table 6. Isotherm parameters for the GLI-Cu²⁺-SSAC adsorption system at 30°C

Langmuir	Values	Freundlich	Values	Temkin	Values
$Q_{m} (mg/g)$	109.21	n_{F}	1.73	A _T (L/mg)	0.99
$K_L(L/mg)$	0.066	$K_F(mg/g)(L/mg)^{1/n}$	10.70	$B_T(L/mg)$	20.23
RMSE	0.70	RMSE	2.62	RMSE	4.01
Error (%)	3.83	Error (%)	11.48	Error (%)	19.56

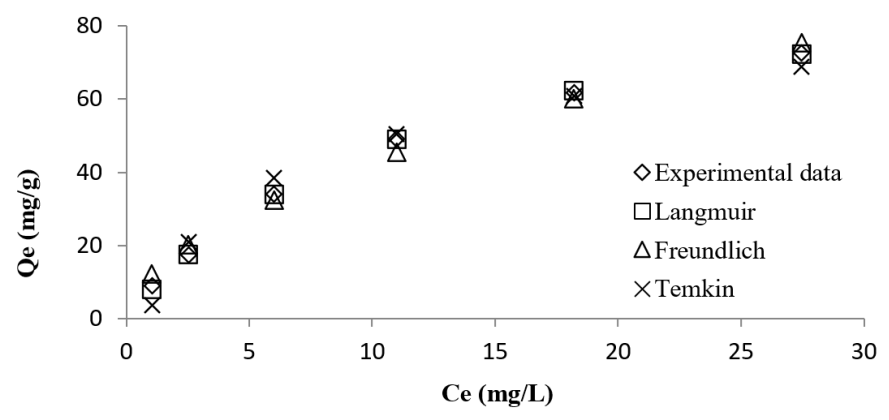


Figure 7. Isotherm plots for the GLI-Cu²⁺-SSAC adsorption system at 30 °C

Conclusion

Cu2+-SSAC was successfully synthesised under conditions derived through specifically at an activation temperature of 587 °C, an activation time of 1.09 h, and a Cu2+ ion IR of 0.50 g/g. Under these conditions, the material achieved a GLI uptake of 70.13 mg/g and a yield of 32.33%. The experimental outcomes closely aligned with the model predictions, exhibiting low relative errors of 2.17% for GLI uptake and 3.26% for yield, thereby validating the robustness of the developed models. Regression analysis showed excellent model accuracy, with high coefficients of determination (R² values) of 0.9648 for the GLI uptake and 0.9311 for Cu2+-SSAC yield. The models also demonstrated low S.D. (2.00 and 1.98) and high A.P. values of 17.51 and 13.26, respectively. According to the ANOVA, the activation temperature and IR were identified as the most influential parameters for both responses. The optimised Cu2+-SSAC exhibited strong textural properties, including a BET-SA of 752.25 m²/g, a MESO-SA of $550.85 \text{ m}^2/\text{g}$, a TPV of $0.3074 \text{ cm}^3/\text{g}$, and an APD of 2.43 nm, confirming its mesoporous nature. SEM imaging further revealed a welldeveloped porous morphology, confirming the efficiency of the activation and modification processes. Isotherm modelling indicated that GLI adsorption on the optimised Cu2+-SSAC followed the Langmuir model, suggesting monolayer adsorption with a Q_m of 109.21 mg/g. These findings highlight the potential of Cu2+-SSAC as an efficient and lowcost adsorbent for pharmaceutical removal from aqueous systems, paving the way for future studies to evaluate its reusability, performance in dynamic systems, and application in treating real wastewater.

Acknowledgement

This investigation is sponsored by the Malaysian Ministry of Higher Education under the Fundamental Research Grant Scheme (project code: FRGS/1/2023/TK05/USM/02/8).

References

- Zaini, Y.M.M., Purba, L.D.A., Abdullah, N., Yuzir, A., Iwamoto, K., and Mohamad, S.E. (2022). Removals of atenolol, gliclazide and prazosin using sequencing batch reactor. *Materials Today: Proceedings*, 65: 3007-3014.
- Mohamad, F.M.Y., Abdullah, A.Z., and Ahmad, M.A. (2024). Amoxicillin adsorption from aqueous solution by Cu(II) modified lemon peel based activated carbon: Mass transfer simulation, surface area prediction and F-test on isotherm and kinetic models. *Powder Technology*, 438.
- 3. Sahin, I., Bakiner, O., Demir, T., Sari, R., and Atmaca, A. (2024). Current position of gliclazide and sulfonylureas in the contemporary treatment paradigm for type 2 diabetes: A scoping review. *Diabetes Therapy*, 15(8): 1687-1716
- Khir, N.H.M., Salleh, N.F.M., Ghafar, N.A., Shukri, N.M., and Jusoh, R. (2025). Preparation and characterization of modified rambutan peels for the removal of chromium(VI) and nickel(II) from aqueous solution: Environmental impact and optimization *Malaysian Journal of Analytical Sciences*, 29(1): 1292.
- Ramlee, D.A., Nordin, N.A., Rahman, N.A., and Bahruji, H. (2024). Removal of acetaminophen by using electrospun pan/sago lignin-based activated carbon nanofibers. *Malaysian Journal* of *Analytical Sciences*, 28(6): 1442-1457.
- Gunasekaran, S., Liu, A.J.X., and Ng, S.L. (2024). Activated carbon/iron oxide composites with different weight ratios for acid orange 7 removal. *Malaysian Journal of Analytical Sciences*, 28(6): 1359-1373.
- Firdaus, M. Y. M., Rashid, M. M., Alam, M. M., and Ahmad, M. A. (2025). Copper-modified surface of orange peel-derived activated carbon for amoxicillin removal: Mass transfer simulation, attraction mechanism, and

- regeneration studies. *Arabian Journal for Science and Engineering*, 2025: 1-23.
- Hatta, N.S.M., Farihahusnah, H., Ti, G.L., and Kheireddine, A.M. (2024). Characterisation of egg white-impregnated activated carbon for CO₂ adsorption application. *Malaysian Journal of Science*, 43: 20-25.
- 9. Yusop, M.F.M., Ahmad, M.A., Rosli, N.A., Gonawan, F.N., and Abdullah, S.J. (2021). Scavenging malachite green dye from aqueous solution using durian peel based activated carbon. *Malaysian Journal of Fundamental and Applied Sciences*, 17(1): 95-103.
- Saputra, D.A., Pratoto, A., Rahman, M.F., and Kodama, A. (2024). The effect of chemical activation agents and activation temperature on the pore structure of rice husk-derived activated carbon. *Malaysian Journal of Science*, 43(Sp1): 1-7
- Ahammad, N. A., Yusop, M. F. M., Mohd Din, A. T., and Ahmad, M. A. (2021). Preparation of alpinia galanga stem based activated carbon via single-step microwave irradiation for cationic dye removal. *Sains Malaysiana*, 50(8): 2251-2269.
- Ahmad, M. A., Yusop, M. F. M., Awang, S., Yahaya, N. K. E. M., Rasyid, M. A. and Hassan, H. (2021). Carbonization of sludge biomass of water treatment plant using continuous screw type conveyer pyrolyzer for methylene blue removal. *IOP Conference Series: Earth and Environmental Science*, 765: 012112.
- 13. Daouda, M.M.A., Akowanou, A.V.O., Mahunon, S.E.R., Adjinda, C.K., Aina, M.P., and Drogui, P. (2021). Optimal removal of diclofenac and amoxicillin by activated carbon prepared from coconut shell through response surface methodology. *South African Journal of Chemical Engineering*. 38(1): 78-89.
- 14. Yusop, M.F.M., Baharudin, M.H., Rashid, M.M., Alam, M.M., and Ahmad, M.A. (2025). Amoxicillin adsorption onto oil palm trunk-derived activated carbon: synthesis optimization, modelling of mass transfer and ultrasonic regeneration. *Journal of Chemical Technology & Biotechnology*, 100(6): 1310-1327.
- Mohamad, F.M.Y., Rashid, M.M., Alam, M.M., and Ahmad, M.A. (2025). Copper metalfunctionalized carbon from rattan waste via microwave pyrolysis for enhanced chloramphenicol removal: Optimization and Ftest study. *Particuology*, 100: 196-213.
- Niam, A.C., Fenelon, E., Ningsih, E., Mirzayanti, Y.W., Kristanti, E., and Naushad, M. (2022). High-efficiency adsorption of hexavalent chromium from aqueous solution by samanea saman activated carbon. *Adsorption Science & Technology*, 2022: 8960379.

- Ni'am, A.C., Suhar, M., Fenelon, E., and Ponnusamy, S.K. (2023). Characterization and potential of *Samanea saman*-activated carbon on adsorption of copper from an aqueous solution. *Adsorption Science & Technology*, 2023: 1911596.
- 18. Naji, S.Z. and Tye, C.T. (2022). A review of the synthesis of activated carbon for biodiesel production: Precursor, preparation, and modification. *Energy Conversion and Management: X.* 13: 100152.
- Almahbashi, N.M.Y., Kutty, S.R.M., Ayoub, M., Noor, A., Salihi, I.U., Al-Nini, A., Jagaba, A.H., Aldhawi, B.N.S., and Ghaleb, A.A.S. (2021). Optimization of preparation conditions of sewage sludge based activated carbon. *Ain Shams Engineering Journal*, 12(2): 1175-1182.
- Rosli, N.A., Ahmad, M.A., and Noh, T.U. (2023). Nature's waste turned savior: Optimizing pineapple peel-based activated carbon for effective Remazol Brilliant Violet dye adsorption using response surface methodology. *Inorganic Chemistry Communications*, 153: 110844.
- 21. Langmuir, I. (1918). The adsorption of gases on plane surfaces of glass, mica and platinum. *Journal of the American Chemical Society*. 40(9): 1361-1403.
- 22. Freundlich, H. (1906). Over the adsorption in solution. *Journal of Physical Chemistry*, 57(385471): 1100-1107.
- 23. Tempkin, M. and Pyzhev, V. (1940). Kinetics of ammonia synthesis on promoted iron catalyst. *Acta Physicochimica URSS*, 12(1): 327.
- 24. Mohamad, F.M.Y., Abdullah, A.Z., and Ahmad, M.A. (2023). Adsorption of remazol brilliant blue R dye onto jackfruit peel based activated carbon: Optimization and simulation for mass transfer and surface area prediction. *Inorganic Chemistry Communications*, 158: 117112.
- 25. Beyan, S.M., Prabhu, S.V., Sissay, T.T., and Getahun, A.A. (2021). Sugarcane bagasse based activated carbon preparation and its adsorption efficacy on removal of BOD and COD from textile effluents: RSM based modeling, optimization and kinetic aspects. *Bioresource Technology Reports*, 14: 100664.
- Yu, H., Mikšík, F., Thu, K., and Miyazaki, T. (2024). Characterization and optimization of pore structure and water adsorption capacity in pinecone-derived activated carbon by steam activation. *Powder Technology*, 431: 119084.
- Weldekidan, H., Patel, H., Mohanty, A., and Misra, M. (2024). Synthesis of porous and activated carbon from lemon peel waste for CO₂ adsorption. *Carbon Capture Science & Technology*, 10: 100149.

- 28. Firdaus, M.Y.M., Nasran, M.N.K., Ridzuan, Z., Zuhairi, A.A., and Azmier, M.A. (2023). Mass transfer simulation on remazol brilliant blue R dye adsorption by optimized teak wood Based activated carbon. *Arabian Journal of Chemistry*, 16(6): 104780.
- Njewa, J.B., Vunain, E., and Biswick, T. (2022). Synthesis and characterization of activated carbons prepared from agro-wastes by chemical activation. *Journal of Chemistry*, 2022(1): 9975444.
- 30. Yusop, M.F.M., Jaya, E.M.J., Din, A.T.M., Bello, O.S., and Ahmad, M.A. (2022). Single-stage optimized microwave-induced activated carbon from coconut shell for cadmium adsorption. *Chemical Engineering & Technology*, 45(11): 1943-1951.
- 31. Firdaus, M.Y.M., Rashid, M.M., Alam, M.M., and Ahmad, M.A. (2025). Enhanced Cd²⁺ removal via deprotonated-mango trunk

- functionalized carbon: Optimization and F-test for linear and non-linear isotherm and kinetic models. *Chemical Engineering Research and Design*, 220: 96-116.
- 32. Wei, X., Huang, S., Yang, J., Liu, P., Li, X., Wu, Y., and Wu, S. (2023). Adsorption of phenol from aqueous solution on activated carbons prepared from antibiotic mycelial residues and traditional biomass. *Fuel Processing Technology*, 242: 107663.
- 33. Aziz, A., Yusop, M.F.M., and Ahmad, M.A. (2024). Harnessing microwave energy to transform *Nephelium lappaceum* L. peel into activated carbon for chloramphenicol eradication in aqueous solutions. *Materials Chemistry and Physics*, 318: 129311.
- 34. Çavuşoğlu, F.C. (2023). Gliclazide removal efficiency of carbon-based magnetic materials: Isotherm and kinetic studies. *Chemical Engineering & Technology*, 46(4): 635-643.